Abl2 is recruited to ventral actin waves through cytoskeletal interactions to promote lamellipodium extension

Ke Zhang[a], Wanqing Lyu[b], Ji Yu[c], and Anthony J. Koleske[b,d,*]
[a]Department of Cell Biology, [b]Department of Molecular Biophysics and Biochemistry, and [d]Department of Neuroscience, Yale University, New Haven, CT 06520; [c]Department of Genetics and Developmental Biology, University of Connecticut Health Center, Farmington, CT 06030

ABSTRACT **Abl family nonreceptor tyrosine kinases regulate changes in cell shape and migration. Abl2 localizes to dynamic actin-rich protrusions, such as lamellipodia in fibroblasts and dendritic spines in neurons. Abl2 interactions with cortactin, an actin filament stabilizer, are crucial for the formation and stability of actin-rich structures, but Abl2:cortactin-positive structures have not been characterized with high spatiotemporal resolution in cells. Using total internal reflection fluorescence microscopy, we demonstrate that Abl2 colocalizes with cortactin at wave-like structures within lamellum and lamellipodium tips. Abl2 and cortactin within waves are focal and transient, extend to the outer edge of lamella, and serve as the base for lamellipodia protrusions. Abl2-positive foci colocalize with integrin β3 and paxillin, adhesive markers of the lamellum–lamellipodium interface. Cortactin-positive waves still form in Abl2 knockout cells, but the lamellipodium size is significantly reduced. This deficiency is restored following Abl2 reexpression. Complementation analyses revealed that the Abl2 C-terminal half, which contains domains that bind actin and microtubules, is necessary and sufficient for recruitment to the wave-like structures and to support normal lamellipodium size, while the kinase domain–containing N-terminal half does not impact lamellipodium size. Together, this work demonstrates that Abl2 is recruited with cortactin to actin waves through cytoskeletal interactions to promote lamellipodium extension.**

Monitoring Editor
Alpha Yap
University of Queensland

Received: Jan 18, 2018
Revised: Aug 28, 2018
Accepted: Sep 19, 2018

INTRODUCTION

Interactions between the actin cytoskeleton and cell surface adhesion complexes are crucial for cell morphogenesis and migration. Extracellular cues activate surface receptors such as integrins to trigger the formation of adhesion structures that directly engage the actin cytoskeleton (Gaus *et al.*, 2006; Legate and Fässler, 2009; Huttenlocher and Horwitz, 2011; Schiller *et al.*, 2013). Additionally, actin polymerization itself can trigger the recruitment of adapter proteins to the cell periphery that initiate the formation of receptor complexes (Nobes and Hall, 1995; Galbraith *et al.*, 2007; Case and Waterman, 2011). One such family of adapter proteins is the Abelson (Abl) nonreceptor tyrosine kinases, comprised of Abl1/c-Abl and Abl2/Arg in vertebrates, which are unique among tyrosine kinases for their ability to bind directly to both the cytoskeleton and cell surface receptors. Abl family kinases directly interact with and phosphorylate numerous cytoskeleton-regulatory proteins including N-WASp, Crk, p190RhoGAP, and cortactin (Kain and Klemke, 2001; Antoku *et al.*, 2008; Greuber *et al.*, 2013; Khatri *et al.*, 2016). These interactions collectively mediate changes in cell shape and movement following growth factor and adhesion receptor engagement (Lewis *et al.*, 1996; Plattner *et al.*, 1999, 2003; Miller *et al.*, 2004; Moresco *et al.*, 2005; Boyle *et al.*, 2007; Mader *et al.*, 2011).

Cortactin is an Arp2/3 complex activator and actin filament stabilizer (Weed *et al.*, 2000; Uruno *et al.*, 2001; Weaver *et al.*, 2002;

This article was published online ahead of print in MBoC in Press (http://www.molbiolcell.org/cgi/doi/10.1091/mbc.E18-01-0044) on September 26, 2018.
The authors have no conflict of interest to disclose.
*Address correspondence to: Anthony J. Koleske (anthony.koleske@yale.edu).
Abbreviations used: Abl, Abelson; EGF, epidermal growth factor; MT, microtubule; sptPALM, single-particle tracking and photoactivated localization microscopy; TIRF, total internal reflection fluorescence.

Head *et al.*, 2003) that supports formation of actin-rich protrusions such as circular dorsal ruffles, lamellipodia, and invadopodia (Krueger *et al.*, 2003; Boyle *et al.*, 2007; Lapetina *et al.*, 2009; Oser *et al.*, 2009). Abl2 and cortactin synergize to promote actin stability and activate the Arp2/3 complex (Courtemanche *et al.* 2015), and both proteins are necessary for dynamic cell edge protrusions in fibroblasts triggered by adhesion to fibronectin or growth factor stimulation (Miller *et al.*, 2004; Boyle *et al.*, 2007; Lapetina *et al.*, 2009; Courtemanche *et al.*, 2015). Abl2 and cortactin interact directly via two distinct binding motifs, and while disruption of these interactions impairs dynamic cell behaviors (Lapetina *et al.*, 2009; Mader *et al.*, 2011), the spatiotemporal dynamics of where Abl2 and cortactin interact in the cell and how this impacts cell morphology have not been well characterized. Understanding the cellular structures generated and modified by Abl2 and cortactin is essential to revealing how these proteins mediate actin-based cell protrusion.

Here, we provide a comprehensive spatiotemporal perspective on the localization of Abl2 and cortactin colocalized to two discrete structures within cell protrusions: at ventral waves marking the lamellum–lamellipodium interface and at the lamellipodial tip. Using two-color total internal reflection fluorescence (TIRF) microscopy in live cells, we found that Abl2 and cortactin colocalize to actin waves at the lamellum–lamellipodium interface and demonstrate that these structures also overlap with integrin β3 and paxillin, but not integrin β1. The appearance of Abl2:cortactin-rich actin waves is associated with dynamic lamellipodia protrusions that extend from the lamella. Using CRISPR/Cas9-mediated knockout of Abl2 and subsequent rescue with full-length Abl2 or truncation mutants, we show that Abl2 C-terminal extension, which contains its cytoskeleton-interacting domains, is necessary and sufficient both for localization to actin waves and to support the formation of full-sized lamellipodium from these waves. These results identify Abl2 as a key organizer of cytoskeletal structure at the lamellum–lamellipodium interface that promotes full lamellipodial formation.

RESULTS

Abl2 and cortactin colocalize with actin at ventral waves at the lamellum–lamellipodium interface

To study Abl2 and cortactin localization in COS-7 cells, we performed immunofluorescence staining of endogenous Abl2, cortactin, and actin. These proteins were enriched in wave-like structures near the cell edge that were visible in epifluorescence mode, but more clearly visible in TIRF mode, indicating close apposition to the cell membrane (Figure 1). Abl2 and cortactin both colocalized with actin at distinct structures at the cell periphery, appearing in a continuous band near the cell edge. The Abl2/cortactin/actin-rich structures resembled actin waves previously described by other groups (Bretschneider *et al.*, 2004, 2009; Gerisch *et al.*, 2004; Case and Waterman, 2011). Unlike actin waves that were observed throughout the cell, however, Abl2- or cortactin-positive ventral waves were only observed at the cell periphery (Figures 1, C and D, and 2).

To visualize the temporal evolution of Abl2 and cortactin-positive structures, we transiently expressed Abl2-GFP and cortactin-RFP in COS-7 cells and performed live two-color TIRF microscopy. Time-lapse movies revealed the dynamic and transient formation of wave-like structures enriched in Abl2 and cortactin near the cell edge (Figure 2, A and B, and Supplemental Movie 1). Consistent with the endogenous staining, Abl2-GFP and cortactin-RFP signals were especially prominent in TIRF mode, indicating their close apposition to the cell membrane. The Abl2:cortactin signals appeared and disappeared as a traveling wave over a period of minutes, with no foci visible after disappearance of the wave (Figure 2, C and D). The wave traveled both around the cell (Figure 2C) and outward from the cell periphery (Figure 2D).

The appearance of Abl2:cortactin-rich waves was spatially and temporally associated with lamellipodial protrusion at the cell edge distal to the Abl2:cortactin-rich waves (Figure 2, D and E, white triangles). Cells exhibit two different zones of actin structures at the cell edge: the lamellipodium and the lamellum (Forscher and Smith, 1988; Svitkina and Borisy, 1999; Ponti, 2004). Lamellipodia are characterized by branched-actin protrusions driven by the Arp2/3 complex that extend from the lamellum (Pollard and Borisy, 2003; Burnette *et al.*, 2011). The lamellum is a more stable, adhesion-rich zone where retrograde actin flow consolidates into stable actin arcs. The lamellum is also characterized by adhesion-mediated force transduction through actin stress fibers (Waterman-Storer and Salmon, 1997; Kaverina *et al.*, 1998; Schaefer *et al.*, 2002). We observed lamellipodia rapidly extend radially from the more stationary waves (Figure 2, D and E, red triangles). In addition to their localization to waves within the lamellum, Abl2 and cortactin localize to the protruding lamellipodial tips (Figure 2E, white triangle). Together, these data reveal two different dynamic Abl2:cortactin-rich structures at the cell periphery: one forming a transient, membrane-apposed wave from which lamellipodia emanate, and another at the distal edge of lamellipodia.

Abl2:cortactin-rich waves differ from circular dorsal ruffles

Previous work demonstrated that Abl2-mediated phosphorylation of cortactin downstream from growth factor receptor signaling promotes formation of circular dorsal ruffles (Boyle *et al.*, 2007). Given the shape of the Abl2:cortactin-rich waves and their localization near the cell edge, we asked whether these structures might provide a base for circular dorsal ruffles. We transfected COS-7 cells with the actin filament probe LifeAct-GFP and cortactin-RFP, plated cells on fibronectin, and induced dorsal ruffles by serum starvation overnight followed by stimulation with media containing 15 nM epidermal growth factor (EGF) for 30 min (Riedl *et al.*, 2008). Cells exhibited circular dorsal ruffles enriched in LifeAct and cortactin that lasted over 30 min (Supplemental Figure 1 and Supplemental Movie 1). Ruffles were prominent when cells were imaged in epifluorescence mode but not observed in TIRF mode, consistent with the location of ruffles to the dorsal side of the cell. This contrasts with the Abl2:cortactin-rich waves described above, where the signal was visible in epifluorescence mode but was far brighter in TIRF mode, indicating that it is a distinct cytoskeletal structure.

Abl2:cortactin-rich actin waves form at the lamellum–lamellipodium interface

A defining feature of lamellipodia is the presence of actin retrograde flow. In contrast, the lamellum is defined as the adherent portion of the cell edge proximal to lamellipodia in migrating epithelial cells (Waterman-Storer and Salmon, 1997; Waterman-Storer *et al.*, 1999; Ponti, 2004). Our observation that Abl2:cortactin-rich waves are associated with lamellipodial protrusions raised the question of where these waves assemble with respect to the lamellum–lamellipodium interface.

To identify lamellipodia, we transiently expressed LifeAct-GFP and cortactin-RFP in COS-7 cells to visualize actin network flow with respect to wave location. Transient cortactin-positive waves appeared at the lamellipodium base and colocalized with LifeAct (Figure 3, A and B). Cortactin-positive waves form predominantly at the lamellum–lamellipodium interface, where actin retrograde flow

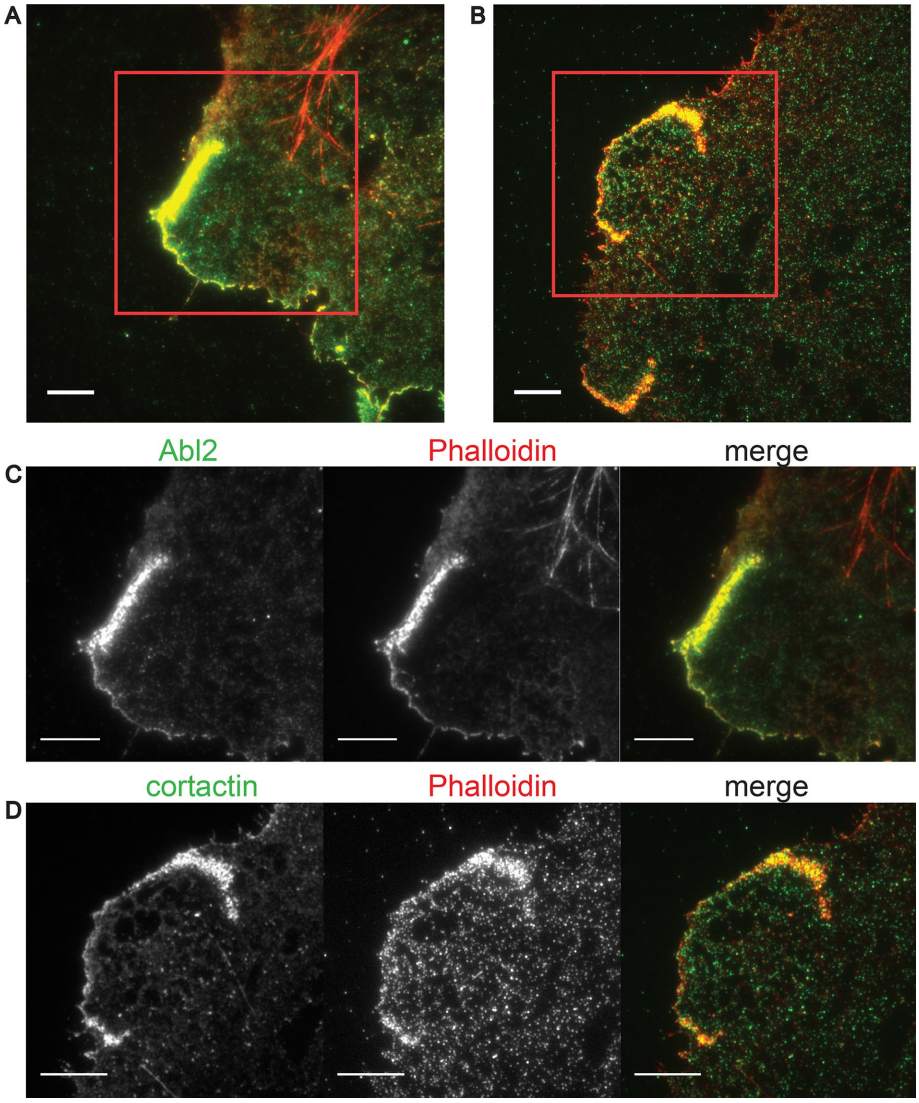

FIGURE 1: Localization of Abl2 and cortactin with actin in COS-7 cells plated on fibronectin. (A–D) COS-7 cells were plated on fibronectin, serum starved, and stimulated with DMEM with 10% FBS for 30 min before fixation and stained using antibodies against endogenous (C) Abl2 (Ar19) and Alexa568-conjugated phalloidin to stain F-actin; (D) cortactin (4F11) and Alexa568-conjugated phalloidin to stain F-actin. (A, B) Uncropped merged images with red box showing the cropped area for C and D. Alexa488 mouse secondary antibody was used to label Abl2 or cortactin. Cell images were acquired in TIRF mode. Scale bar = 10 μm.

stops (Supplemental Movie 2 and Figure 3B, red dashed lines). The appearance of a new cortactin signal within the lamellipodium evolved over time into the new location of the lamellum–lamellipodium interface further distal from the cell center (Figure 3B, white triangle).

We also assessed the localization of Abl2 and cortactin relative to the lamellum–lamellipodium interface by visualizing microtubules (MTs), which extend within lamella but do not penetrate into lamellipodia (Waterman-Storer and Salmon, 1997; Kaverina *et al.*, 1998, 1999). We used the MT plus tip marker GFP-MACF43 to visualize MT extension from the cell center to cell lamella (Figure 3, C and D; Yau *et al.*, 2016). GFP-MACF43–labeled MT plus tips neither extended beyond the Abl2- or cortactin-positive waves nor moved into growing lamellipodia. Together, these findings suggest that Abl2:cortactin-positive waves form at the lamellum–lamellipodium interface.

Abl2:cortactin-rich actin waves colocalize with integrin β3 and paxillin at the lamellum–lamellipodium interface but not with integrin β1

The appearance of Abl2:cortactin-rich waves on the cell membrane at the lamellum–lamellipodium interface suggests that these structures may interact with membrane receptor complexes. We plated COS-7 cells and immunostained for Abl2 or cortactin and various membrane receptors and associated proteins. Using immunofluorescence microscopy, we found that Abl2 and cortactin in waves colocalize with integrin β3 and paxillin (Figure 4, A and B), both markers of nascent adhesions and focal complexes (Zaidel-Bar *et al.*, 2003; Scales and Parsons, 2011). Although previous genetic and biochemical studies have shown that Abl2 interacts with integrin β1 (Warren *et al.*, 2012; Simpson *et al.*, 2015), we did not observe significant colocalization of Abl2 or cortactin with integrin β1 (Figure 4, C and D). Unbiased quantification of colocalization using Pearson's coefficient demonstrate significantly higher colocalization of Abl2 and cortactin to integrin β3 than to integrin β1 (Figure 4E).

To further examine spatiotemporal dynamics of colocalization, we performed live-cell imaging of COS-7 cells expressing Abl2-RFP and paxillin-GFP (Figure 4, F and G). Paxillin colocalized with Abl2 at small punctate foci at the lamellum–lamellipodium interface in regions that exhibited lamellipodia protrusions (Supplemental Movie 3 and Figure 4G, white triangles).

Abl2 molecules exhibit two diffusional states and the slower diffusion state predominates in waves

Because Abl2:cortactin-rich waves colocalize with membrane receptor complexes, we asked whether these complexes alter the motion of Abl2 at the cell membrane. Imaging Abl2:cortactin-rich ventral waves at 2 s intervals revealed that the waves are composed of multiple separate foci (Supplemental Movie 4). We sought to test whether Abl2 at these foci was freely diffusing or more constrained, consistent with association with a higher order complex.

We used single-particle tracking and photoactivated localization microscopy (sptPALM) to track Abl2-mEOS3.2 single-particle trajectories (Figure 5 and Supplemental Movie 6; Manley *et al.*, 2008; Oh *et al.*, 2012; Rossier *et al.*, 2012; Zhang *et al.*, 2012). Abl2 molecule trajectories were visualized as single Abl2 molecules appearing at the cell membrane, diffusing, and disappearing due to either loss of the Abl2-mEOS3.2 molecule from the TIRF plane or its photobleaching. Within each frame of a movie, we utilized Gaussian fitting algorithms to localize the positions of individual Abl2-mEOS3.2 molecules to subdiffraction-limited resolution (Jaqaman *et al.*, 2008; Mortensen *et al.*, 2010; Huang *et al.*, 2013). Particle coordinates from consecutive frames of a movie

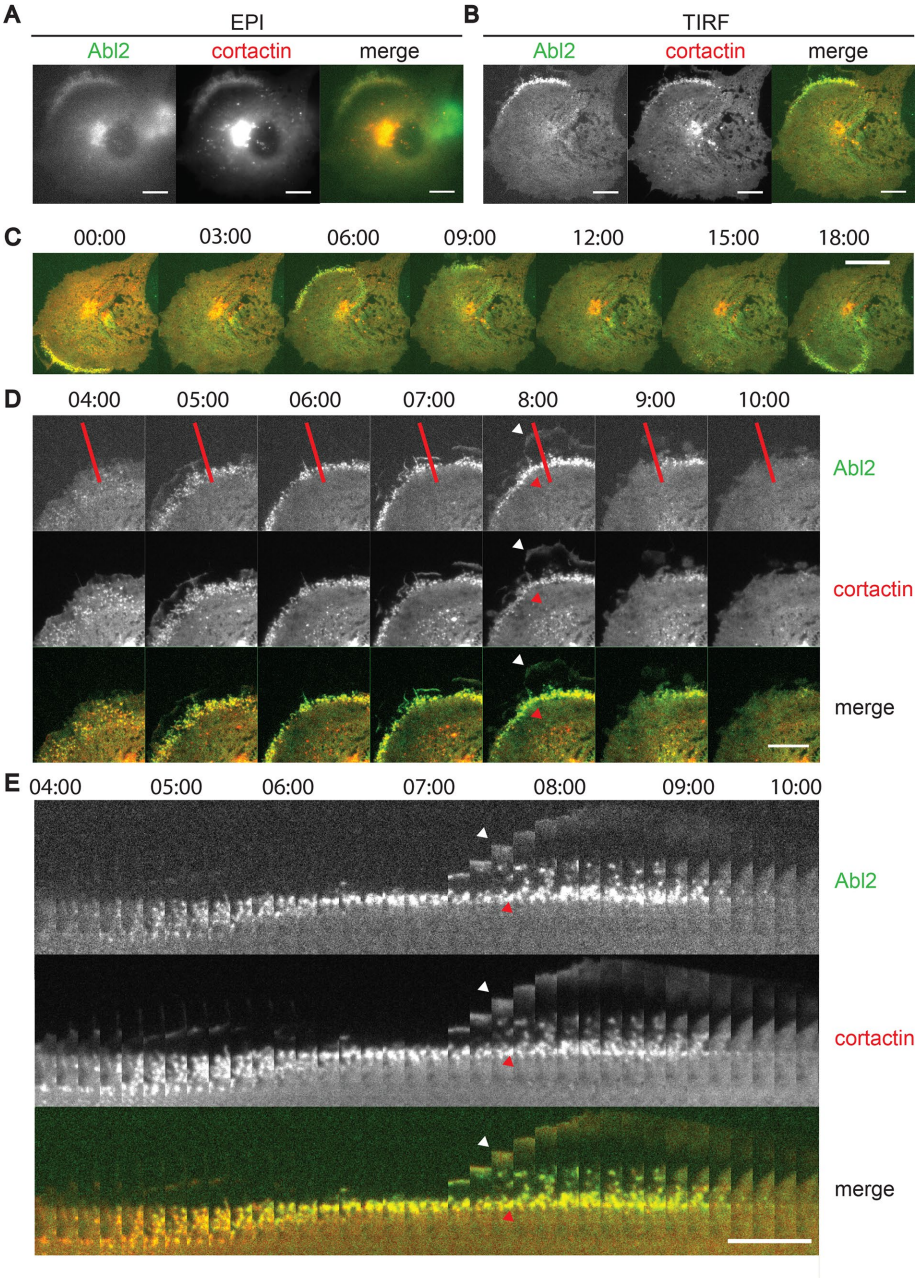

FIGURE 2: Abl2 and cortactin colocalize in dynamic ventral waves at the cell periphery associated with lamellipodia. (A, B) Time-lapse fluorescence images of COS-7 cell expressing Abl2-GFP and cortactin-RFP plated on 10 μg/ml fibronectin. Images adapted from Supplemental Movie 1, which was acquired over 20 min at 10 s intervals in 488 and 561 nm excitations using alternating Epi mode and TIRF mode. Scale bar = 10 μm. (A) Images of Abl2-GFP, cortactin-RFP, and merge in Epi mode. (B) Images from same the same movie as A in TIRF mode. (C) Montage of Supplemental Movie 1 in TIRF mode where slices are taken 3 min apart. Scale bar = 10 μm. (D) Montage of Supplemental Movie 1 in TIRF mode where slices are taken at 1-min intervals. Scale bar = 10 μm. White triangle indicates lamellipodium edge. Red triangle indicates lamellum. (E) Montage of Supplementql Movie 1 taken at the cell location indicated by the red bar in D. Slices are 10 s apart. Scale bar = 10 μm. White triangle indicates lamellipodium edge. Red triangle indicates lamellum.

were connected using nearest-neighbor algorithms to assemble a single-molecule trajectory.

We first performed TIRF imaging of nonphotoconverted total Abl2-mEOS3.2 in the green channel to define an Abl2-rich wave region of interest. We then compared single Abl2-mEOS3.2 molecule behavior within regions of interest containing waves and outside of the waves. Analyses of single-step displacements revealed a two-Gaussian distribution, indicating two diffusional states (Figure 5, D and E). Further analysis using hidden Markov modeling on assembled trajectories revealed the fraction of Abl2 molecules behaving in high versus low diffusional state. Abl2 within waves exhibited a larger proportion of molecules in the lower diffusion state, consistent with their possible interactions with larger structures within the waves (Figure 5F).

Abl2 C-terminal cytoskeleton-interacting domains are sufficient for localization to waves

We next examine which of Abl2's domains (e.g., kinase, cytoskeleton-binding) mediate its interactions with membrane structures at waves. Like Src family nonreceptor tyrosine kinases, Abl family kinases contain tandem SH3, SH2, and kinase domains in their N-terminal halves. Their extended C-termini are unique to Abl family kinases (Figure 6A). The Abl2 C-terminal half, which contains two actin-binding domains, a MT-binding domain, and a PxxP motif that binds the cortactin SH3 domain, is necessary and sufficient for the formation of dynamic cell edge protrusions in fibroblasts (Lapetina *et al.*, 2009; Liu *et al.*, 2012). The Abl2-ΔC mutant containing the SH3-SH2-kinase module but lacking the C-terminal extension remained cytoplasmic and did not colocalize with cortactin at the waves (Figure 6B and Supplemental Movie 4). However, the C-terminal Abl2-557-C construct colocalized with cortactin at foci within Abl2:cortactin-rich waves (Figure 6C and Supplemental Movie 5). Quantification revealed that Abl2-557-C colocalized with cortactin at levels comparable to wild-type (WT) Abl2, while Abl2-ΔC did not colocalize with cortactin. These data suggest that the Abl2 C-terminal extension is necessary and sufficient to localize Abl2 to the Abl2:cortactin-rich actin waves.

Knocking out Abl2 decreases lamellipodia size adjacent to Abl2:cortactin-positive waves

We next examined whether and how the loss of Abl2 function impacted ventral actin waves or lamellipodial extension. Control parental COS-7 cells exhibited an average wave lifetime of 10.1 ± 1.6 min, with waves traveling an average of 6.1 ± 1.2 μm radially from the nucleus (Figure 7). Lamellipodia associated with waves were an average of 2.2 ± 0.2 μm in radial width as measured from the distal edge of the lamellum base to the lamellipodial tip (Figure 7, C, white triangles, and G).

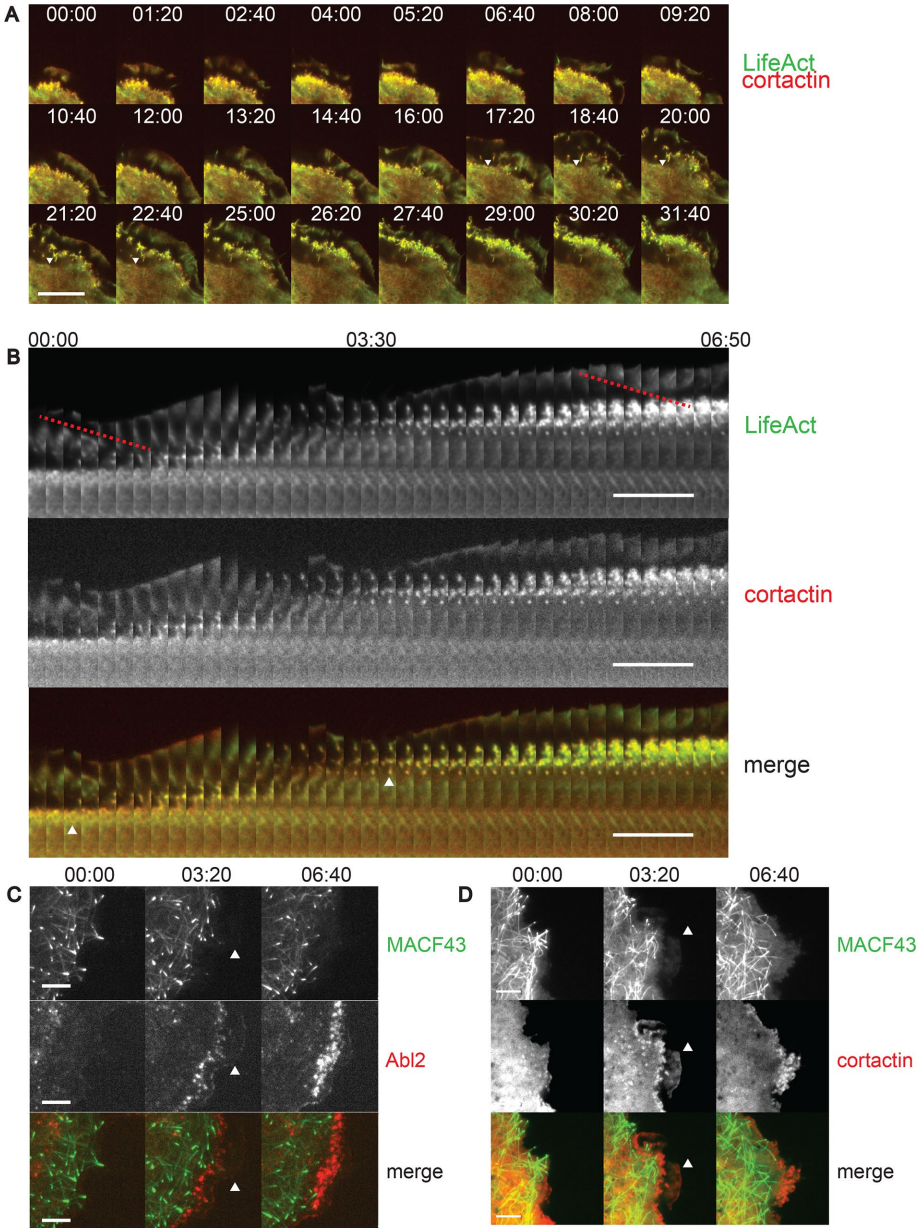

FIGURE 3: Abl2:cortactin-rich waves occur at the lamellum–lamellipodium border and corresponds with lamellum extension. (A) LifeAct and cortactin colocalize at wave-like structures. Montage shows the colocalization of cortactin and LifeAct signals as they move peripherally. Triangle indicates the appearance of new cortactin:LifeAct-positive foci that mark a new outer boundary of the lamellum–lamellipodium interface. (B) Montage showing cortactin-positive wave forming new lamellum and triggering new lamellipodia (white triangles). Kymograph adapted from Supplemental Movie 2, which was acquired in TIRF mode with slices taken 10 s apart. Total time is 6 min and 50 s. Scale bar = 10 µm. (C) Microtubule plus tips do not extend beyond the Abl2-RFP waves. Time-lapse TIRF images from Supplemental Movie 2 showing COS-7 cells transfected with GFP-MACF43 and Abl2-RFP plated on fibronectin. Triangle indicates outer edge of lamellipodia. Scale bar = 5 µm. (D) Microtubule plus tips do not extend beyond the cortactin-RFP waves. Time-lapse TIRF images from Supplemental Movie 4 showing COS-7 cells transfected with GFP-MACF43 and cortactin-RFP plated on fibronectin. Triangle indicates outer edge of lamellipodia. Scale bar = 5 µm.

Waves in Abl2-KO COS-7 cells, generated using CRISPR/Cas9 editing with >92% loss of Abl2 expression in the cell population (Supplemental Figure 2) were visualized with LifeAct-GFP and cortactin-RFP (Figure 7B). Knocking out Abl2 did not impact the average wave lifetime and did not change the average radial distance traveled by waves (10.1 ± 1.56 min WT vs. 13.6 ± 1.7 min Abl2-KO, $p = 0.14$; 6.1 ± 1.2 µm WT vs. 6.5 ± 1.1 µm, $p = 0.84$; Figure 7, H and I). However, Abl2-KO cells exhibited significantly smaller lamellipodia distal to the waves, decreasing from an average of 2.2 ± 0.2 µm to 0.9 ± 0.1 µm in radial length (Figure 7, E–G).

Reexpression of WT Abl2 or the Abl2-557-C fragment containing the Abl2 C-terminal cytoskeleton-interacting domains in Abl2 KO cells restored lamellipodia sizes to those observed in WT cells (2.2 ± 0.22 µm in control cells, 1.8 ± 0.2 µm in Abl2 rescued Abl2KO cells, and 2.1 ± 0.2 µm in Abl2-557-C rescued Abl2 rescued Abl2KO cells; Figure 7, E, F, and J, and Supplemental Figure 2). However, rescuing with Abl2-ΔC fragment containing just the SH3, SH2, and kinase domain induced a slight increase in lamellipodial size over Abl2 KO cells that was not statistically significant (0.9 ± 0.1 µm in Abl2-KO and 1.3 ± 0.2 µm in Abl2-ΔC rescue, $p = 0.08$; Figure 7, G and J). These data show that Abl2 is not necessary for wave formation at the cell periphery, but that loss of Abl2 function significantly decreased lamellipodium size.

DISCUSSION

We present evidence that Abl2 and cortactin colocalize with actin at ventral waves at the cell periphery. Abl2:cortactin waves form at the lamellum–lamellipodium interface and marks sites from which lamellipodia emanate. The Abl2:cortactin-rich waves also colocalize with paxillin and integrin β3, known markers of focal complexes found at the lamellum–lamellipodial interface. Using Abl2 knockout and complementation with Abl2 or mutants thereof, we show that Abl2 employs its C-terminal domain to localize to waves and promote lamellipodium size.

Comparison of Abl2:cortactin-rich waves to similar structures in other biological contexts

Many different actin-rich wave-like structures have been described previously, including circular dorsal ruffles, actin waves, and other membrane receptor–mediated signaling waves (Vicker, 2002; Bretschneider *et al.*, 2004; Gerisch *et al.*, 2004; Weiner *et al.*, 2007; Case and Waterman, 2011; Azimifar *et al.*, 2012). Abl2 and cortactin have also been previously localized to circular dorsal ruffles (Krueger *et al.*, 2003; Boyle *et al.*, 2007). The actin-rich waves we describe form on the ventral cell surface and consist of puncta enriched in Abl2 and cortactin.

Abl2:cortactin-rich waves are similar to the actin waves described in *Dictyostelium* cells by Gerisch *et al.* (2004) because they are actin-rich, adjacent to the cell edge, and persist for many minutes.

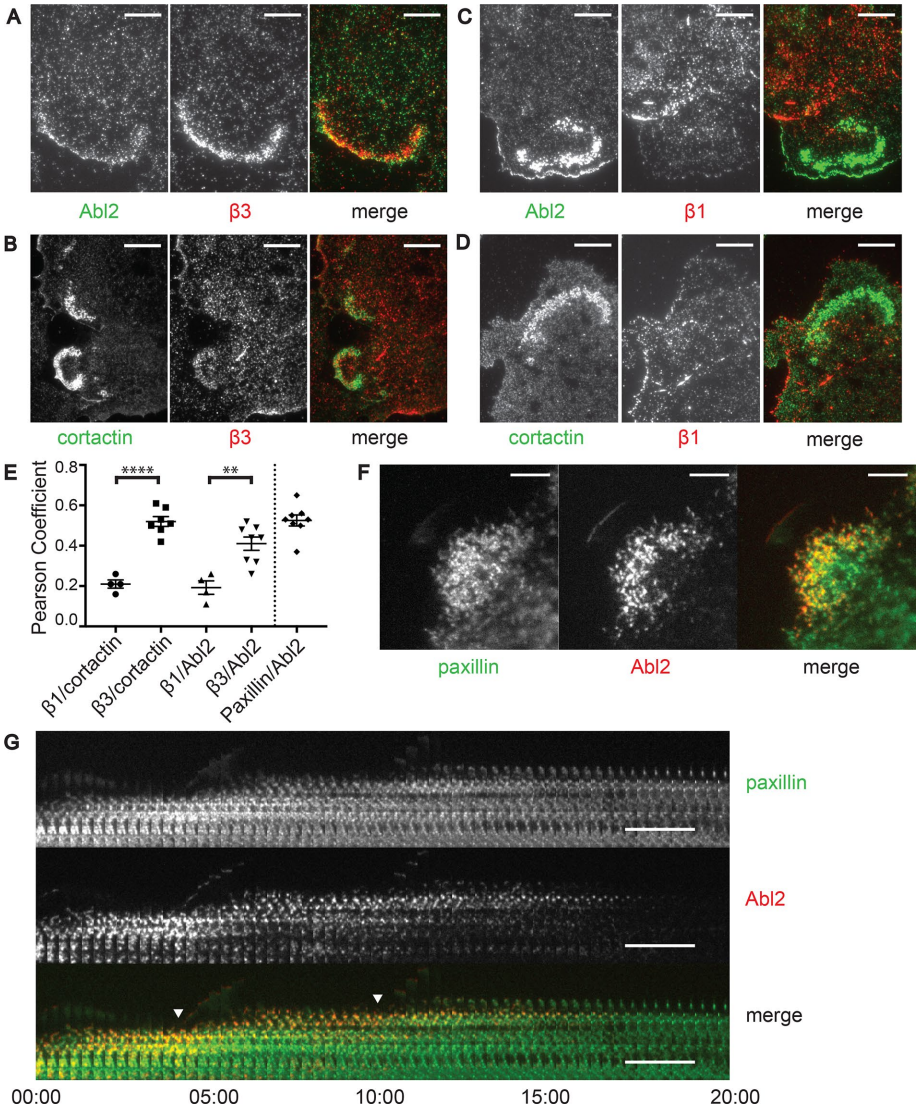

FIGURE 4: Abl2:cortactin foci colocalize with paxillin and integrin β3 in actin waves. (A, B) Image showing COS-7 cells fixed and stained using antibodies against endogenous Abl2 (Ar19) or cortactin (4F11) and β3 integrin (Millepore; clone EPR2417Y). Scale bar = 10 μm. (C, D) Image showing COS-7 cells fixed and stained using antibodies against endogenous Abl2 (Ar19) or cortactin (4F11) and β1 integrin (Millepore; MAB1965). Scale bar = 10 μm. (E) Pearson's coefficient quantifying colocalization of Abl2 or cortactin with β3 integrin, Abl2 or cortactin with β1 integrin, and of Abl2 with paxillin. Each value is taken from one image from one cell. Error bars represent SEM. $N = 4$ cells each for β1/cortactin and β1/Abl2. $N = 8$ cells each for β3/cortactin and β3/Abl2 and paxillin/Abl2. β3/cortactin colocalization is statistically higher than β1/cortactin; $p < 0.0001$. β3/Abl2 colocalization is statistically higher than β1/Abl2; $p = 0.0022$. (F) Abl2 and paxillin colocalize at actin waves at the cell periphery. Representative image from TIRF Supplemental Movie 3 where COS-7 cells are transfected with paxillin-GFP and Abl2-RFP and plated on fibronectin. (G) Kymographic analysis of the cell edge taken from Supplemental Movie 3, where slices are taken 20 s apart, showing appearance of Abl2 and paxillin signals at the cell edge. Triangle indicates formation of a new lamellipodium. Scale bar = 10 μm.

However, unlike the waves in *Dictyostelium*, the Abl2:cortactin waves appear on small sections of the cell edge, rarely spanning a large portion of the overall cell circumference. Abl2:cortactin-rich waves do not form a closed loop, at least not proximal to the membrane, but appear and disappear as crescent waves approaching the cell edge. This progression is more similar to the actin waves described by Case and Waterman in U2OS human osteosarcoma cells, where integrin-mediated adhesion complex signaling propagates on the ventral surface of a cell until it hits a cell edge (Case and Waterman, 2011). In this context, Arp2/3-mediated branched-actin waves precede recruitment of adhesion complex proteins such as VASP, zyxin, and paxillin followed by a wave of integrin activation. Here we note that Abl2 and cortactin synergistically stabilize actin filaments and activate Arp2/3-mediated actin branching, and these functions may be their main roles at actin waves (Courtemanche *et al.*, 2015). Case and Waterman (2011) report actin-rich waves throughout the ventral attached surface of the cell, whereas we find Abl2:cortactin-rich waves predominantly occur at the cell periphery and are associated with the lamellum–lamellipodium interface. It remains possible that Abl2:cortactin-rich waves are the end result of ventral actin waves hitting adhesion complexes such as focal complexes. Therefore, one potential role for Abl2:cortactin recruitment to actin waves is to amplify Arp2/3-mediated actin branching near sites of focal complex formation to modulate the actin structure near the cell edge.

Reducing Abl2 in cells decreases lamellipodia size, which can be rescued with an Abl2 C-terminal fragment

Quantification of lamellipodia lifetime, distance traveled, and average radial width demonstrate that Abl2 promotes larger lamellipodia but does not affect lamellipodial lifetime and distance traveled. Furthermore, rescuing Abl2 knockout cells with the Abl2 C-terminal fragment is sufficient to restore lamellipodia sizes, whereas the N-terminal kinase domain fragment does not. These findings are consistent with previous work in fibroblasts showing that Abl2 C-terminal domains play a kinase-independent scaffolding role in cell edge protrusions (Lapetina *et al.*, 2009). It is interesting that the N-terminal domain is not sufficient to localize to waves, considering that this fragment is capable of directly binding membrane receptors such as integrins β1 and β3 (Warren *et al.*, 2012; Simpson *et al.*, 2015). Further, SH3-SH2 domains of related kinases such as Src have been shown to mediate interactions with membrane complexes (Machiyama *et al.*, 2015). One possibility is that Abl2 SH3-SH2–kinase domain is predominantly in an autoinhibited state and relies on the C-terminal cytoskeletal domains for recruitment to the correct cellular structures (Hantschel *et al.*, 2003). This could explain why Abl2 preferentially colocalizes with integrin β3 versus integrin β1 while in vitro pull-down experiments show that Abl2 N-terminal fragment binds integrin β1 more strongly (Warren *et al.*, 2012). Future work is needed to determine the role of Abl2 kinase activity, if any, at actin waves and at the leading edge of lamellipodia.

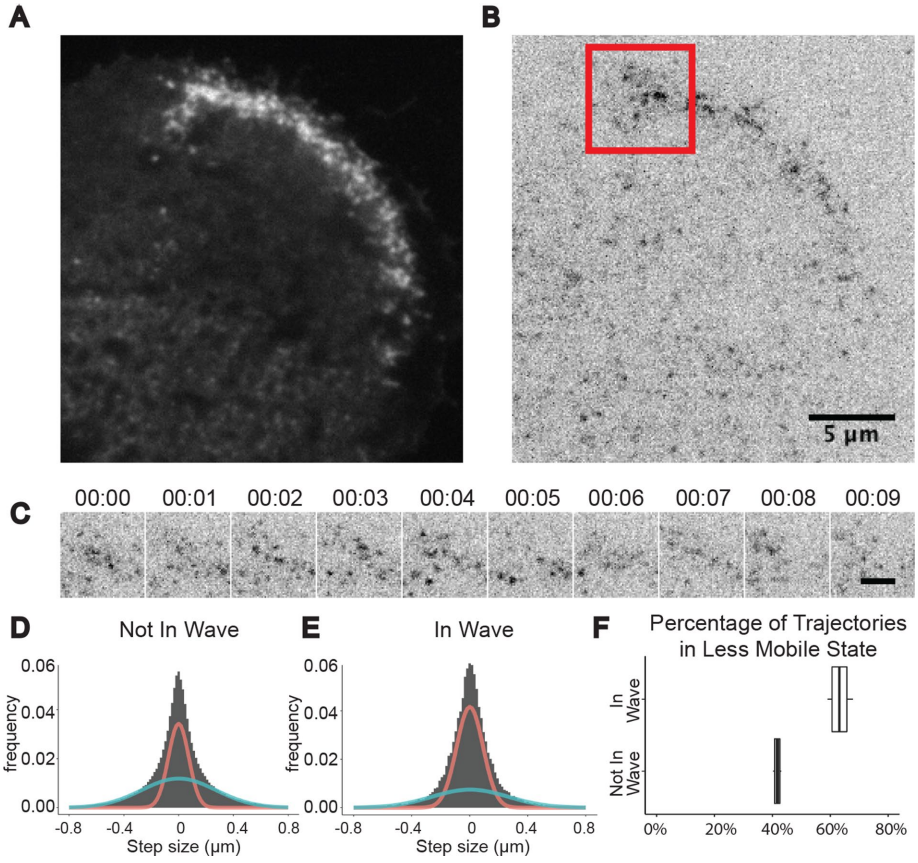

FIGURE 5: sptPALM analyses reveal Abl2 diffuses slower in waves than outside of waves. (A) Image of an Abl2-mEOS3.2 wave captured in TIRF mode at 561 nm to visualize all Abl2-mEOS3.2. (B) Representative image of Abl2-mEOS3.2 from Supplemental Movie 6 with background subtracted and color inverted showing localization to actin waves at the cell periphery. Scale bar = 5 µm. (C) Kymograph generated from the Abl2-mEOS3.2 Supplemental Movie using the red box crop shown in B. Although the kymograph is shown at 1 s intervals, the actual Abl2-mEOS3.2 Supplemental Movie was acquired at 100 ms exposures. (D, E) Single-step distribution of tracked Abl2 molecule trajectories between two consecutive frames of the movie showing that the overall distribution is the sum of two-Gaussian distributions; 25,000 single steps were sampled in the histogram. Red and blue Gaussian curves represent fitted populations by mixture analysis. Fitting done on pooled trajectories collected from 10 movies, each from a different cell. (D) Abl2 molecules from the whole cell surface without waves were identified and tracked. (E) Abl2 molecules inside a region of interest around active waves were identified and tracked. (F) Box-and-whisker plot of population distribution from hidden Markov modeling of trajectories showing fraction of trajectories categorized as less mobile. Box indicates 95% confidence interval on the posterior distribution fitting.

Abl2:cortactin-rich waves are transiently associated with focal complexes at the lamellum–lamellipodium interface

Because Abl2:cortactin-rich waves are seen only at the cell periphery, they may be selectively recruited by transient cell adhesions found at the lamellum–lamellipodium interface known as focal complexes (Nobes and Hall, 1995; Zaidel-Bar *et al.*, 2003; Burdisso *et al.*, 2013). Focal complexes are rich in integrin β3, paxillin, FAK, and other adapter proteins in addition to actin and MTs (Scales and Parsons, 2011). These complexes may serve as binding sites to recruit Abl2 molecules, consistent with Abl2 single-particle tracking data demonstrating a preference for confined diffusion within actin waves. It is of note that integrin-mediated adhesions are among the most potent activators of Abl family kinases (Lewis and Schwartz, 1998; Li and Pendergast, 2011; Simpson *et al.*, 2015) and integrin β3 cytoplasmic tail can bind to Abl2 kinase directly, albeit with lower affinity than integrin β1. However, our data suggest that Abl2 localizes to actin wave complexes primarily through transient cytoskeletal interactions rather than direct engagement of surface receptors. Movies of cells expressing paxillin and Abl2 revealed that Abl2 dissociates before paxillin, indicating that Abl2 only briefly localizes to the paxillin-positive focal complexes. The preferential interaction with specific cytoskeletal structures may explain why Abl2:cortactin-rich puncta do not also undergo myosin-II–dependent maturation of focal complexes into focal adhesions (Choi *et al.*, 2008; Schneider *et al.*, 2009).

Abl2:cortactin-rich waves mark sites of dynamic lamellipodial protrusions

Abl2 and cortactin are necessary for the formation of actin-based cell edge protrusions (Krueger *et al.*, 2003; Miller *et al.*, 2004; Lapetina *et al.*, 2009). We show here that Abl2 and cortactin localize to the lamellum–lamellipodium interface and to the tip of lamellipodia. Abl2:cortactin waves appear to mark sites of lamellipodia protrusions. This is consistent with past work showing the importance of adhesion-dependent actin changes for cell migration (Burnette *et al.*, 2014; Swaminathan *et al.*, 2016; Barnhart *et al.*, 2017). In addition, Abl2 and cortactin localize in a thin band at the very tip of growing lamellipodia. Interestingly, Abl2:cortactin foci neither dislodge from the lamellipodia tip nor exhibit retrograde flow backwards. Therefore, Abl2 and cortactin may primarily interact with actin at the leading edge and release as the actin network undergoes retrograde flow (Burnette *et al.*, 2011; Ryan *et al.*, 2012). These data reveal for the first time two distinct Abl2:cortactin complexes: one found at the lamellum–lamellipodium interface that serves as the base of expanding lamellipodia, and one at the leading edge of lamellipodia.

MATERIALS AND METHODS

Molecular cloning

Murine Abl2, cortactin, and paxillin cDNA were cloned into pN1 expression vectors with indicated fluorescent protein tags using *Xho*1 and *Age*1 cut sites. Abl2 mutants were generated by PCR as described previously (Miller *et al.*, 2004). LifeAct was cloned into pN1 vector with EGFP as described previously (Riedl *et al.*, 2008). mEOS3.2 photo-switchable fluorophore was replaced by the fluorophore in pN1-EGFP expression vector using *Age*1 and *Not*1 cut sites (Zhang *et al.*, 2012). GFP-MACF43 was described previously (Yau *et al.*, 2016).

Cell culture and construct transfection

Mycoplasma-free COS-7 cells were purchased from the American Type Culture Collection and grown in DMEM supplemented with 10% fetal bovine serum (FBS), 100 U/ml penicillin, 100 µg/ml

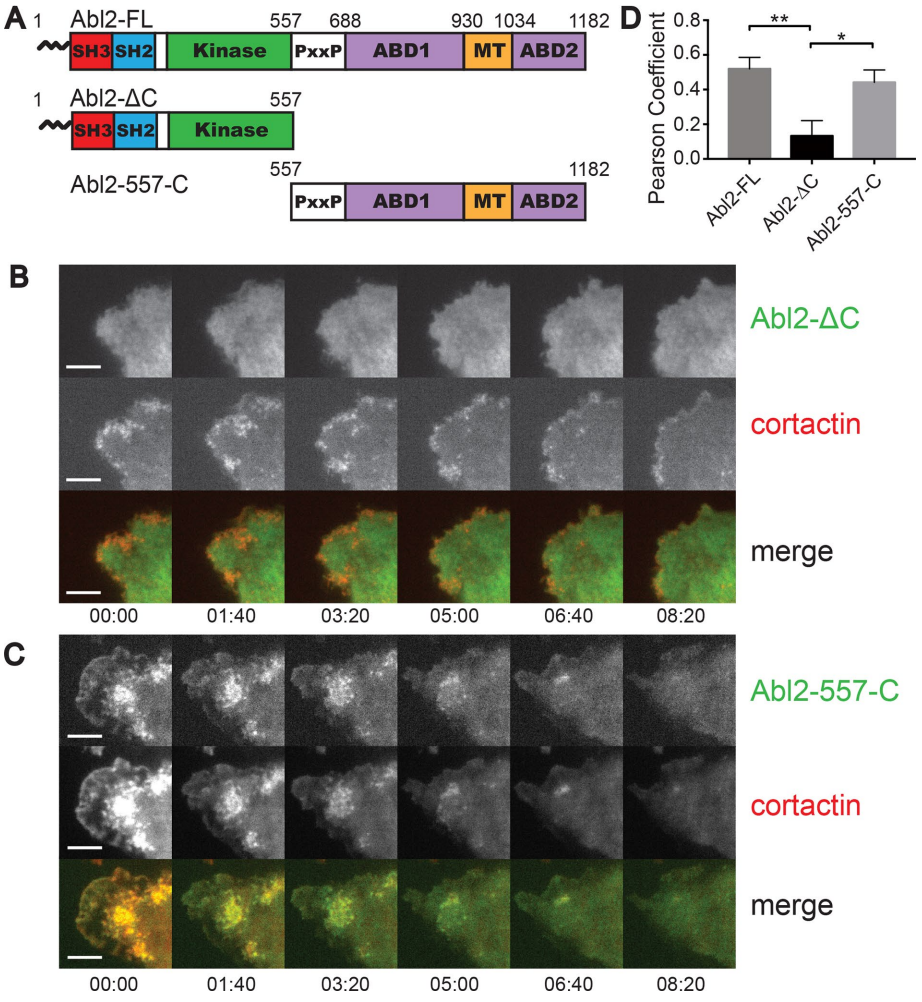

FIGURE 6: The Abl2 C-terminal half is sufficient for colocalization with cortactin at ventral waves. (A) Domain structure of Abl2 full length (Abl2-FL), Abl2 with C-terminal cytoskeleton domains deleted (Abl2-ΔC), and Abl2 with the N-terminal SH3-SH2–kinase cassette deleted (Abl2-557-C). (B, C) Abl2-ΔC mutant does not colocalize with cortactin at actin waves. (B) Images from TIRF Supplemental Movie 4 showing Abl2-ΔC-GFP, cortactin-RFP, and composite. Scale bar = 5 μm. (C) Images from TIRF Supplemental Movie 5 showing Abl2-557-C-GFP, cortactin-RFP, and composite. Scale bar = 5 μm. (D) Quantification of Pearson coefficient of colocalization between Abl2-FL-GFP, Abl2-ΔC-GFP, or Abl2-557-C-GFP with cortactin-RFP. Error bar represents SEM. $N = 6$ cells for each condition. $p = 0.0212$ between Abl2-ΔC-GFP and Abl2-557-C-GFP, and $p = 0.0054$ between Abl2-ΔC-GFP and Abl2-FL-GFP.

streptomycin, and 2 mM L-glutamine. Cells were transfected with polyethylenimine (Longo *et al.*, 2013) or Lipofectamine 3000 (Thermo Fisher) 24–48 h before imaging according to the manufacturer's instructions. Poly-D-lysine and fibronectin were purchased from Sigma.

Time-lapse live-cell microscopy

Cells were imaged on 30 mm #1.5 coverslips in an interchangeable dish (Bioptechs). Coverslips were plasma cleaned for 4 min using Ar/O_2 and 2 min with H_2/O_2. Coverslips were coated with 50 μg/ml poly-D-lysine for 20 min at room temperature and 10 μg/ml fibronectin in phosphate-buffered saline (PBS) for 1 h at 37°C and blocked with 1% bovine serum albumin (BSA) in PBS for 1 h at 37°C. Cells were seeded at 100,000 cells per coverslip. Live-cell microscopy was performed on a Nikon Ti-E microscope with a 100× TIRF objective (NA = 1.49), an Andor Zyla 4.2 sCMOS camera, and Nikon Elements software. The microscope was equipped with a perfect focus system and automated TIRF angle motor. Cell dishes were maintained at 37°C in a heated chamber, and the objective was warmed using a heating collar (Warner Instruments). Cells were cultured in phenol red-free DMEM supplemented with 10% FBS and 20 mM HEPES (pH 7.3). Excitation was performed with a 405, 488, or 561 nm laser, as appropriate. For live-cell time-lapse movies, the Zyla 4.2 camera was binned at 2 × 2 pixels and acquisitions were performed with 400 ms integration times. Images were acquired in epifluorescence and TIRF mode every 10 s or in TIRF mode every 2 s.

Immunofluorescence microscopy

COS-7 cells were plated on glass coverslips functionalized and coated with 10 μg/ml fibronectin as described above. Cells were serum starved overnight and stimulated with DMEM with 10% FBS for 30 min then fixed with 2% paraformaldehyde/4% sucrose in PBS for 5 min at room temperature. Cells were permeabilized with blocking buffer (0.1% Triton X-100, 3% BSA, 2% FBS in PBS) for 1 h. Abl2-specific mouse antibody (Ar19), cortactin-specific mouse antibody (4F11), or β3 integrin rat antibody (Millipore; clone EPR2417Y) were used at 1:100 dilutions. Alexa488 anti-mouse secondary antibody from Invitrogen was used at 1:1000. Alexa568 rabbit antibody was used to label β3 integrin. Alexa568-conjugated phalloidin was used at 1:100 (Thermo Fisher). All antibodies were diluted in blocking buffer.

Generation of Abl2 knockout cell lines by CRISPR/Cas9-mediated genome editing

Abl2 knockout cos7 cells were generated using CRPISPR/Cas9 as described by the Zhang lab (Shalem *et al.*, 2014). Briefly, a 20–base pairs guide sequence (5′-GAGAAAGTGAGAGTAGCCCT-3′) with an adjacent PAM (GGG) targeting the fourth exon of Abl2 was inserted into lentiCRISPR plasmid. HEK293T cells were transfected with the constructed lentiCRISPR plasmid, packaging plasmid psPAX2, and envelope plasmid pCMV-VSV-G, to generate lentivirus. Control parental Cos7 cells were infected with the generated lentivirus. The Abl2 selected with 2 μg/ml puromycin for 72 h and the cell lysates were collected for immunoblot to determine the expression level of Abl2. Abl2 KO cells exhibited >92% loss of Abl2 signal by blotting with Ar11 and Ar19.

Western blot analysis

Cells were lysed with 1× LSB buffer (8% SDS, 20% glycerol, 100 mM Tris, pH = 6.8, 8% 2-mercaptoethanol, and complete protease inhibitors) at 95°C. A polyacrylamide gel was prepared, and lysates were run at 120 V for 1.5 h. Protein was then transferred to nitrocellulose paper, blocked using the 5% milk and immunoblotted with Ar11, which recognizes Abl2 C-terminus (residues 766–1182), and Ar19, which recognizes Abl2 N-terminus (both antibodies were a kind gift from Peter Davies, Albert Einstein Medical College,

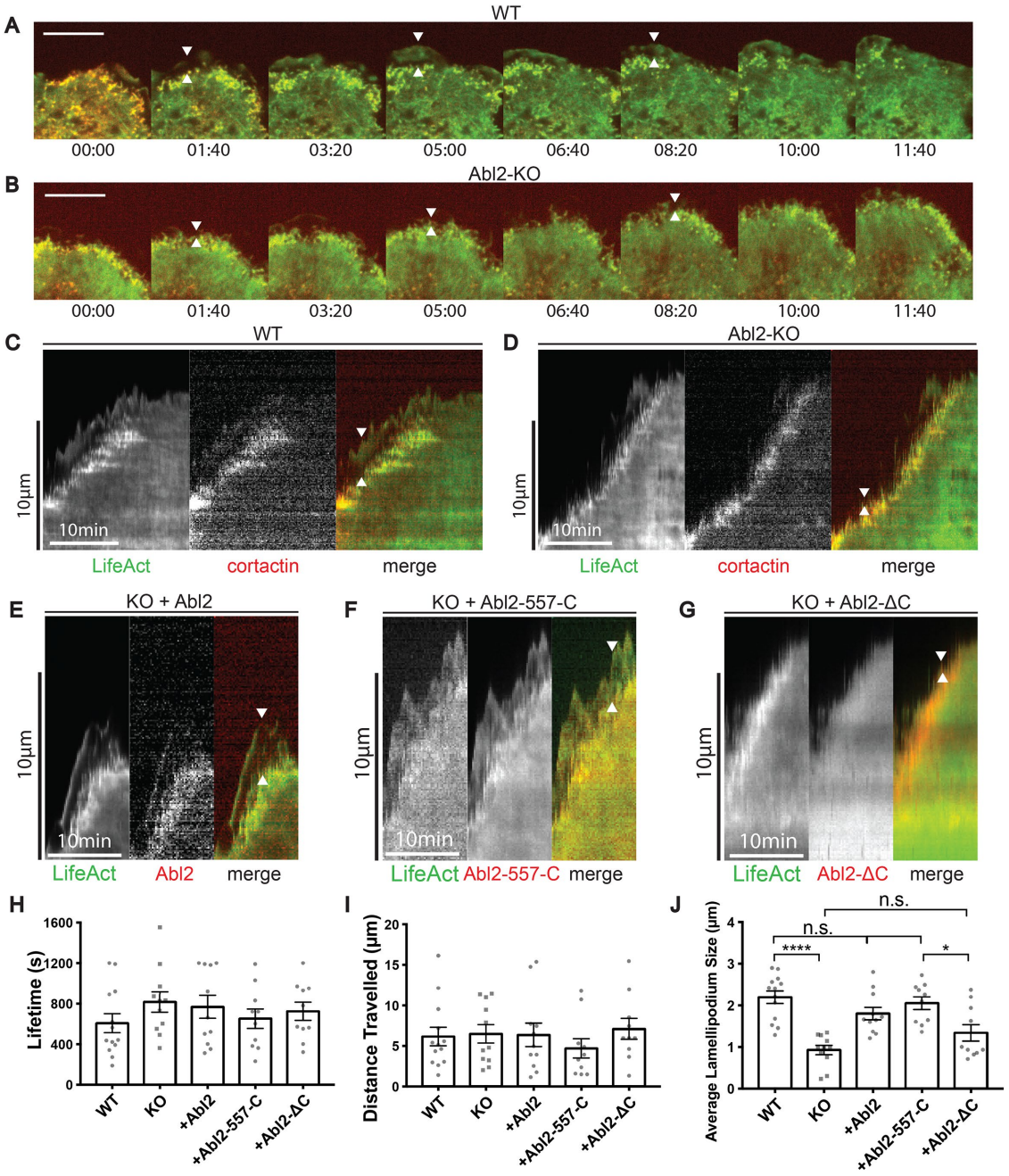

FIGURE 7: Knocking out Abl2 does not affect wave lifetime or distance traveled but decreases lamellipodia size. (A, B) Merged montage images of WT or Abl2-KO cells expressing LifeAct-GFP and cortactin-RFP. Images adapted from Supplemental Movie 7, which were acquired at 10 s intervals in 488 and 561 nm excitations in TIRF mode. Scale bar = 10 µm. (C–G) Single-line kymographs where *x*-axis is time and *y*-axis is length. Scale bars as indicated. (C, D) Kymographs acquired from Supplemental Movie 7. (E–G) Kymographs acquired from Supplemental Movie 8, which were acquired at 10 s intervals in 488 and 561 nm excitations in TIRF mode. COS7 Abl2-KO cells rescued with Abl2-RFP, Abl2-ΔC-RFP, or Abl2-557-C-RFP and LifeAct-GFP. Scale bar = 10 µm. (H–J) Quantification of wave behavior in wild-type COS7 cells (WT; $n = 13$), COS7 cells with Abl2 knocked out (KO; $n = 11$), and Abl2-KO COS7 cells transfected with full-length Abl2 ($n = 11$), Abl2-557-C ($n = 10$), or Abl2-ΔC ($n = 10$). Each *n* is one wave in one cell. Error bars equal SEM. (H) Quantification of wave lifetime in seconds. (I) Quantification of distance traveled by wave in micrometers. (J) Quantification of average lamellipodium size exhibited by wave over the lifetime of the wave. **** indicates $p < 0.0001$. * indicates $p = 0.011$.

Bronx, NY). Quantitation of protein expression was performed by measuring the intensity of each band in background-subtracted images in ImageJ, using the intensity of ponceau S stain image for each lane as the loading control.

Single-particle tracking and hidden Markov model analysis

mEos3.2-tagged molecules were fluorescently excited using a 561 nm laser with the laser power at 20 W/cm^2 coming out of the objective in Epi mode. Cells were photoswitched using a 500 ms

pulse of 405 nm laser at 2.5 W/cm^2. Subsequently, movies were acquired using 100 ms integration time continuously. Using custom written software in Matlab, R, and ImageJ, fluorescent dots corresponding to single molecules were identified by intensity thresholding and the positions were tracked over time using the nearest-neighbor method. For single-step distribution analysis, trajectories were segmented into individual displacements and pooled. A total of 5000 single steps were used to distribution analysis. The subsequent distribution was fitted using Gaussian mixture fitting. Full trajectory analysis of single molecules using hidden Markov modeling was performed as described previously (Das *et al.*, 2009). Briefly, we used the displacements of single-molecule steps in a trajectory as a Markov chain and employed a Bayesian Hamiltonian Monte Carlo algorithm to regress the data to two diffusion constant states and two transition rates between the two states. Diffusion rates from the single-step Gaussian analysis were used for Monte Carlo analysis. This analysis allows us to extract the steady-state distributions of Abl2 molecules in each diffusion state. The Hamiltonian Monte Carlo algorithm was utilized using the STAN modeling language through the RStan interface (Carpenter *et al.*, 2017). Monte Carlo simulations were performed on clusters at Yale's Center for Research Computing. Source code for analysis is available upon request.

Statistical analyses

Analyses were performed with unpaired, two-tailed *t* tests, as appropriate. Significance was defined as $p < 0.05$. Error bars represent SEM. Calculations were performed using GraphPad Prism or R.

ACKNOWLEDGMENTS

We thank Xianyun Ye for providing technical assistance and Aaron Levy, Alexander Scherer, Mitchell Omar, Juliana Shaw, and Sara Katrancha for feedback on the manuscript. This work was supported by National Institutes of Health (NIH) Grants no. NS-089662, no. NS-105640, and no. MH-115939 to A.J.K., no. F30CA-19289902 to K.Z., and Cellular and Molecular Biology Training grant no. T32GM007223 to Susan Baserga.

REFERENCES

Antoku S, Saksela K, Rivera GM, Mayer BJ (2008). A crucial role in cell spreading for the interaction of Abl PxxP motifs with Crk and Nck adaptors. J Cell Sci 121, 3071–3082.

Azimifar SB, Böttcher RT, Zanivan S, Grashoff C, Krüger M, Legate KR, Mann M, Fässler R (2012). Induction of membrane circular dorsal ruffles requires co-signalling of integrin–ILK-complex and EGF receptor. J Cell Sci 125, 435–448.

Barnhart EL, Allard J, Lou SS, Theriot JA, Mogilner A (2017). Adhesion-dependent wave generation in crawling cells. Curr Biol 27, 27–38.

Boyle SN, Michaud GA, Schweitzer B, Predki PF, Koleske AJ (2007). A critical role for cortactin phosphorylation by Abl-family kinases in PDGF-induced dorsal-wave formation. Curr Biol 17, 445–451.

Bretschneider T, Anderson K, Ecke M, Müller-Taubenberger A, Schroth-Diez B, Ishikawa-Ankerhold HC, Gerisch G (2009). The three-dimensional dynamics of actin waves, a model of cytoskeletal self-organization. Biophys J 96, 2888–2900.

Bretschneider T, Diez S, Anderson K, Heuser J, Clarke M, Müller-Taubenberger A, Köhler J, Gerisch G (2004). Dynamic actin patterns and Arp2/3 assembly at the substrate-attached surface of motile cells. Curr Biol 14, 1–10.

Burdisso JE, Gonzalez A, Arregui CO (2013). PTP1B promotes focal complex maturation, lamellar persistence and directional migration. J Cell Sci 126, 1820–1831.

Burnette DT, Shao L, Ott C, Pasapera AM, Fischer RS, Baird MA, Der Loughian C, Delanoe-Ayari H, Paszek MJ, Davidson MW, *et al.* (2014). A contractile and counterbalancing adhesion system controls the 3D shape of crawling cells. J Cell Biol 205, 83–96.

Burnette DT, Manley S, Sengupta P, Sougrat R, Davidson MW, Kachar B, Lippincott-Schwartz J (2011). A role for actin arcs in the leading-edge advance of migrating cells. Nat Cell Biol 13, 371–382.

Carpenter B, Gelman A, Hoffman MD, Lee D, Goodrich B, Betancourt M, Brubaker M, Guo J, Li P, Riddell A (2017). Stan: A probabilistic programming language. J Stat Soft 76, 1–32.

Case LB, Waterman CM (2011). Adhesive F-actin waves: a novel integrin-mediated adhesion complex coupled to ventral actin polymerization. PLoS One 6, e26631.

Choi CK, Vicente-Manzanares M, Zareno J, Whitmore LA, Mogilner A, Horwitz AR (2008). Actin and α-actinin orchestrate the assembly and maturation of nascent adhesions in a myosin II motor-independent manner. Nat Cell Biol 10, 1039–1050.

Courtemanche N, Gifford SM, Simpson MA, Pollard TD, Koleske AJ (2015). Abl2/Abl-related gene stabilizes actin filaments, stimulates actin branching by actin-related protein 2/3 complex, and promotes actin filament severing by cofilin. J Biol Chem 290, 4038–4046.

Das R, Cairo CW, Coombs D (2009). A hidden Markov model for single particle tracks quantifies dynamic interactions between LFA-1 and the actin cytoskeleton. PLoS Comput Biol 5, e1000556.

Forscher P, Smith SJ (1988). Actions of cytochalasins on the organization of actin filaments and microtubules in a neuronal growth cone. J Cell Biol 107, 1505–1516.

Galbraith CG, Yamada KM, Galbraith JA (2007). Polymerizing actin fibers position integrins primed to probe for adhesion sites. Science 315, 992–995.

Gaus K, Le Lay S, Balasubramanian N, Schwartz MA (2006). Integrin-mediated adhesion regulates membrane order. J Cell Biol 174, 725–734.

Gerisch G, Bretschneider T, Müller-Taubenberger A, Simmeth E, Ecke M, Diez S, Anderson K (2004). Mobile actin clusters and traveling waves in cells recovering from actin depolymerization. Biophys J 87, 3493–3503.

Greuber EK, Smith-Pearson P, Wang J, Pendergast AM (2013). Role of ABL family kinases in cancer: from leukaemia to solid tumours. Nat Rev Cancer 13, 559–571.

Hantschel O, Nagar B, Guettler S, Kretzschmar J, Dorey K, Kuriyan J, Superti-Furga G (2003). A myristoyl/phosphotyrosine switch regulates c-Abl. Cell 112, 845–857.

Head JA, Jiang D, Li M, Zorn LJ, Schaefer EM, Parsons JT, Weed SA (2003). Cortactin tyrosine phosphorylation requires Rac1 activity and association with the cortical actin cytoskeleton. Mol Biol Cell 14, 3216–3229.

Huang F, Hartwich TMP, Rivera-Molina FE, Lin Y, Duim WC, Long JJ, Uchil PD, Myers JR, Baird MA, Mothes W, *et al.* (2013). Video-rate nanoscopy using sCMOS camera-specific single-molecule localization algorithms. Nat Methods 10, 653–658.

Huttenlocher A, Horwitz AR (2011). Integrins in cell migration. Cold Spring Harb Perspect Biol 3, a005074.

Jaqaman K, Loerke D, Mettlen M, Kuwata H, Grinstein S, Schmid SL, Danuser G (2008). Robust single-particle tracking in live-cell time-lapse sequences. Nat Methods 5, 695–702.

Kain KH, Klemke RL (2001). Inhibition of cell migration by Abl family tyrosine kinases through uncoupling of Crk-CAS complexes. J Biol Chem 276, 16185–16192.

Kaverina I, Rottner K, Small JV (1998). Targeting, capture, and stabilization of microtubules at early focal adhesions. J Cell Biol 142, 181–190.

Khatri A, Wang J, Pendergast AM (2016). Multifunctional Abl kinases in health and disease. J Cell Sci 129, 9–16.

Krueger EW, Orth JD, Cao H, McNiven MA (2003). A dynamin-cortactin-Arp2/3 complex mediates actin reorganization in growth factor-stimulated cells. Mol Biol Cell 14, 1085–1096.

Lapetina S, Mader CC, Machida K, Mayer BJ, Koleske AJ (2009). Arg interacts with cortactin to promote adhesion-dependent cell edge protrusion. J Cell Biol 185, 503–519.

Legate KR, Fässler R (2009). Mechanisms that regulate adaptor binding to beta-integrin cytoplasmic tails. J Cell Sci 122, 187–198.

Lewis JM, Schwartz MA (1998). Integrins regulate the association and phosphorylation of paxillin by c-Abl. J Biol Chem 273, 14225–14230.

Lewis JM, Baskaran R, Taagepera S, Schwartz MA, Wang JY (1996). Integrin regulation of c-Abl tyrosine kinase activity and cytoplasmic-nuclear transport. Proc Natl Acad Sci USA 93, 15174–15179.

Li R, Pendergast AM (2011). Arg kinase regulates epithelial cell polarity by targeting β1-integrin and small GTPase pathways. Curr Biol 21, 1534–1542.

Liu W, MacGrath SM, Koleske AJ, Boggon TJ (2012). Lysozyme contamination facilitates crystallization of a heterotrimeric cortactin-Arg-lysozyme

complex. Acta Crystallogr, Sect F: Struct Biol Cryst Commun 68, 154–158.
Longo PA, Kavran JM, Kim M-S, Leahy DJ (2013). Transient mammalian cell transfection with polyethylenimine (PEI). Methods Enzymol 529, 227–240.
Machiyama H, Yamaguchi T, Sawada Y, Watanabe TM, Fujita H (2015). SH3 domain of c-Src governs its dynamics at focal adhesions and the cell membrane. FEBS J 282, 4034–4055.
Mader CC, Oser M, Magalhaes MAO, Bravo-Cordero JJ, Condeelis J, Koleske AJ, Gil-Henn H (2011). An EGFR-Src-Arg-cortactin pathway mediates functional maturation of invadopodia and breast cancer cell invasion. Cancer Res 71, 1730–1741.
Manley S, Gillette JM, Patterson GH, Shroff H, Hess HF, Betzig E, Lippincott-Schwartz J (2008). High-density mapping of single-molecule trajectories with photoactivated localization microscopy Nat Methods 5, 155–157.
Miller AL, Wang Y, Mooseker MS, Koleske AJ (2004). The Abl-related gene (Arg) requires its F-actin–microtubule cross-linking activity to regulate lamellipodial dynamics during fibroblast adhesion. J Cell Biol 165, 407–419.
Moresco EMY, Donaldson S, Williamson A, Koleske AJ (2005). Integrin-mediated dendrite branch maintenance requires Abelson (Abl) family kinases. J Neurosci 25, 6105–6118.
Mortensen KI, Churchman LS, Spudich JA, Flyvbjerg H (2010). Optimized localization analysis for single-molecule tracking and super-resolution microscopy. Nat Methods 7, 377–381.
Nobes CD, Hall A (1995). Rho, rac, and cdc42 GTPases regulate the assembly of multimolecular focal complexes associated with actin stress fibers, lamellipodia, and filopodia. Cell 81, 53–62.
Oh D, Ogiue-Ikeda M, Jadwin JA, Machida K, Mayer BJ, Yu J (2012). Fast rebinding increases dwell time of Src homology 2 (SH2)-containing proteins near the plasma membrane. Proc Natl Acad Sci USA 109, 14024–14029.
Oser M, Yamaguchi H, Mader CC, Bravo-Cordero JJ, Arias M, Chen X, DesMarais V, van Rheenen J, Koleske AJ, Condeelis J (2009). Cortactin regulates cofilin and N-WASp activities to control the stages of invadopodium assembly and maturation. J Cell Biol 186, 571–587.
Plattner R, Irvin BJ, Guo S, Blackburn K, Kazlauskas A, Abraham RT, York JD, Pendergast AM (2003). A new link between the c-Abl tyrosine kinase and phosphoinositide signalling through PLC-γ1. Nat Cell Biol 5, 309–319.
Plattner R, Kadlec L, DeMali KA, Kazlauskas A, Pendergast AM (1999). c-Abl is activated by growth factors and Src family kinases and has a role in the cellular response to PDGF. Genes Dev 13, 2400–2411.
Pollard TD, Borisy GG (2003). Cellular motility driven by assembly and disassembly of actin filaments. Cell 112, 453–465.
Ponti A (2004). Two distinct actin networks drive the protrusion of migrating cells. Science 305, 1782–1786.
Riedl J, Crevenna AH, Kessenbrock K, Yu JH, Neukirchen D, Bista M, Bradke F, Jenne D, Holak TA, Werb Z, *et al*. (2008). Lifeact: a versatile marker to visualize F-actin. Nat Methods 5, 605–607.
Rossier O, Octeau V, Sibarita J-B, Leduc C, Tessier B, Nair D, Gatterdam V, Destaing O, Albigès-Rizo C, Tampé R, *et al*. (2012). Integrins β1 and β3 exhibit distinct dynamic nanoscale organizations inside focal adhesions. Nat Cell Biol 14, 1057–1067.
Ryan GL, Watanabe N, Vavylonis D (2012). A review of models of fluctuating protrusion and retraction patterns at the leading edge of motile cells. Cytoskeleton (Hoboken) 69, 195–206.
Scales TM, Parsons M (2011). Spatial and temporal regulation of integrin signalling during cell migration. Curr Opin Cell Biol 23, 562–568.
Schaefer AW, Kabir N, Forscher P (2002). Filopodia and actin arcs guide the assembly and transport of two populations of microtubules with unique dynamic parameters in neuronal growth cones. J Cell Biol 158, 139–152.
Schiller HB, Hermann M-R, Polleux J, Vignaud T, Zanivan S, Friedel CC, Sun Z, Raducanu A, Gottschalk K-E, Théry M, *et al*. (2013). β1- and αv-class integrins cooperate to regulate myosin II during rigidity sensing of fibronectin-based microenvironments. Nat Cell Biol 15, 625–636.
Schneider IC, Hays CK, Waterman CM (2009). Epidermal growth factor-induced contraction regulates paxillin phosphorylation to temporally separate traction generation from de-adhesion. Mol Biol Cell 20, 3155–3167.
Shalem O, Sanjana NE, Hartenian E, Shi X, Scott DA, Mikkelson T, Heckl D, Ebert BL, Root DE, Doench JG, *et al*. (2014). Genome-scale CRISPR-Cas9 knockout screening in human cells. Science 343, 84–87.
Simpson MA, Bradley WD, Harburger D, Parsons M, Calderwood DA, Koleske AJ (2015). Direct interactions with the integrin β1 cytoplasmic tail activate the Abl2/Arg kinase. J Biol Chem 290, 8360–8372.
Svitkina TM, Borisy GG (1999). Arp2/3 complex and actin depolymerizing factor/cofilin in dendritic organization and treadmilling of actin filament array in lamellipodia. J Cell Biol 145, 1009–1026.
Swaminathan V, Fischer RS, Waterman CM (2016). The FAK-Arp2/3 interaction promotes leading edge advance and haptosensing by coupling nascent adhesions to lamellipodia actin. Mol Biol Cell 27, 1085–1100.
Uruno T, Liu J, Zhang P, Fan Y-X, Egile C, Li R, Mueller SC, Zhan X (2001). Activation of Arp2/3 complex-mediated actin polymerization by cortactin. Nat Cell Biol 3, 259–266.
Vicker MG (2002). F-actin assembly in Dictyostelium cell locomotion and shape oscillations propagates as a self-organized reaction-diffusion wave. FEBS Lett 510, 5–9.
Warren MS, Bradley WD, Gourley SL, Lin Y-C, Simpson MA, Reichardt LF, Greer CA, Taylor JR, Koleske AJ (2012). Integrin β1 signals through Arg to regulate postnatal dendritic arborization, synapse density, and behavior. J Neurosci 32, 2824–2834.
Waterman-Storer CM, Salmon ED (1997). Actomyosin-based retrograde flow of microtubules in the lamella of migrating epithelial cells influences microtubule dynamic instability and turnover and is associated with microtubule breakage and treadmilling. J Cell Biol 139, 417–434.
Waterman-Storer CM, Worthylake RA, Liu BP, Burridge K, Salmon ED (1999). Microtubule growth activates Rac1 to promote lamellipodial protrusion in fibroblasts. Nat Cell Biol 1, 45–50.
Weaver AM, Heuser JE, Karginov AV, Lee W-L, Parsons JT, Cooper JA (2002). Interaction of cortactin and N-WASp with Arp2/3 complex. Curr Biol 12, 1270–1278.
Weed SA, Karginov AV, Schafer DA, Weaver AM, Kinley AW, Cooper JA, Parsons JT (2000). Cortactin localization to sites of actin assembly in lamellipodia requires interactions with F-actin and the Arp2/3 complex. J Cell Biol 151, 29–40.
Weiner OD, Marganski WA, Wu LF, Altschuler SJ, Kirschner MW (2007). An actin-based wave generator organizes cell motility. PLoS Biol 5, e221.
Yau KW, Schatzle P, Tortosa E, Pages S, Holtmaat A, Kapitein LC, Hoogenraad CC (2016). Dendrites in vitro and in vivo contain microtubules of opposite polarity and axon formation correlates with uniform plus-end-out microtubule orientation. J Neurosci 36, 1071–1085.
Zaidel-Bar R, Ballestrem C, Kam Z, Geiger B (2003). Early molecular events in the assembly of matrix adhesions at the leading edge of migrating cells. J Cell Sci 116, 4605–4613.
Zhang M, Chang H, Zhang Y, Yu J, Wu L, Ji W, Chen J, Liu B, Lu J, Liu Y, *et al*. (2012). Rational design of true monomeric and bright photoactivatable fluorescent proteins. Nat Methods 9, 727–729.